

Promising Directions in Chemical Processing of Methane from Coal Industry. Part 2. Development of Catalysts

E.V. Matus*, M.A. Kerzhentsev, A.P. Nikitin, S.A. Sozinov, Z.R. Ismagilov

Federal Research Center of Coal and Coal Chemistry, Siberian Branch, RAS, 18, pr. Sovetskiy, Kemerovo, Russia

Article info

Received:

2 March 2023

Received in revised form:

28 April 2023

Accepted:

14 May 2023

Keywords:

Ni catalyst

Promoter

Nanoparticles

Coal methane

Reforming

Synthesis gas

Abstract

For the creation of new highly active and stable catalysts for the complete processing of coal methane, different methods for designing catalytic systems are being applied, including the use of the effects of mutual strengthening of the action of metals and modifying the composition of the supports. Different chemical synthesis approaches were considered for obtaining supported Ni nanoparticles with controllable compositions and sizes. For the citrate sol-gel method, it was found that with an increase in the citric acid/metals molar ratio from 0 to 1, the textural characteristics (specific surface area: 76→100 m²/g) of Ce_{0.2}Ni_{0.8}O_{1.2}/Al₂O₃ catalysts, dispersion (average particle size: 10→5 nm) and reducibility (temperature of maximum H₂ consumption: 580→530 °C) of the Ni-containing species improved. For calcined in air at 500 °C catalysts it was shown that Ni²⁺ cations stabilized in NiO or in the Ce-Ni-O solid solution. The proportion of the latter was maximum at a citric acid/metal molar ratio equal to 0.25, which was chosen as the optimal value in the investigated range of 0.25–1.0. An increase in the calcination temperature from 500 to 900 °C contributes to the stabilization of Ni²⁺ in the Al-Ni-O solid solution, which leads to a slight deterioration in the textural properties of the samples and a significant difficulty in their reducibility. After reductive activation at 800 °C of Ce_{0.2}Ni_{0.8}O_{1.2}/Al₂O₃ samples, catalytically active metal Ni⁰ nanoparticles of ~7 nm in size were formed for effective reforming of coal industry methane into synthesis gas.

1. Introduction

Coal is a solid, combustible sedimentary rock, formed mainly from dead plants as a result of their biochemical, physicochemical and physical changes. It is an important fuel and energy resource and a valuable raw material for the chemical industry. Despite the fact that the global development strategy assumes a reduction in coal consumption, its share in electricity generation remains at a high level of 37% [1]. The decrease in demand for coal in the EU countries, dictated by the course toward

the decarbonization of the economy and the transition to cleaner sources of electricity generation, is offset by an increase in its consumption in China and Southeast Asia. To achieve a compromise between environmental requirements and economic feasibility, the search for new opportunities for the further development of the coal industry is an urgent task. An effective solution to this issue can be the wider use of coal and associated coal gas as raw materials for the chemical industry.

Coal deposits contain huge reserves of gas hydrocarbon raw materials. The origin of coal bed gas can be biogenic, thermogenic, or mixed. The biogenic gas of coal seams is formed during the decomposition of coal macromolecules to methane

*Corresponding author.

E-mail address: matus_e@mail.ru

as a result of the activity of methanogenic microorganisms at relatively low temperatures ($\sim 50\text{ }^{\circ}\text{C}$) [2–4]. It is believed that gas of biogenic origin is contained in coals with a low degree of coalification. Such deposits, as a rule, are characterized by a low content of methane per ton of coal 4–6 m^3/t . Thermogenic gas is formed from the organic matter of coal as a result of chemical decomposition and thermal cracking reactions during coalification at temperatures above $100\text{ }^{\circ}\text{C}$ without the participation of microorganisms [3, 5, 6]. The intensity of the gas formation depends on the stage of coalification, temperature and pressure. The gas of thermogenic origin accompanies coal deposits with a high degree of coalification. In this case, the methane content in coal reaches high values of 15–20 m^3/t [7].

The composition of coal industry gas depends on the characteristics of the coal deposit, the production stage of coal mining, and varies from day to day. There are four main types of coal industry gases differing in methane content:

(1) VAM – Ventilation Air Methane. Methane from the ventilation air of underground mines. Methane concentration: less than 1 vol.%.

(2) CMM – Coal Mine Methane. Underground mine degassing systems remove gas from coal seams to prevent gas from entering the mine workings of active mines. Methane concentration: 25–60 vol.%;

(3) AMM – Abandoned Mine Methane. Methane from abandoned coal mines. During its extraction by means of degassing, methane concentration may be 60–80 vol.%;

(4) CBM – Coal Bed Methane. Methane from unrelieved coal beds extracted during preliminary degassing through boreholes drilled from the surface. Methane concentration: more than 80 vol.%.

Unlike natural gas, all types of methane-containing gas of the coal industry contain, in addition to methane, air, water vapor, traces of carbon dioxide. Each type of methane-containing gas of the coal industry requires its own optimal disposal path. In the first stage of our investigations the thermodynamic analysis of the main reactions going on in the multicomponent system $\text{CH}_4\text{--CO}_2\text{--H}_2\text{O--air}$ is carried out [8]. The possibility of 100% methane conversion is demonstrated, along with the possibility to obtain hydrogen-containing gas with the concentration 40 to 90 vol.% using the methane-air mixture from coal production. For the processing

of a methane-air mixture of variable composition with a methane concentration of 30–80%, the most promising are the methods of catalytic combined reforming (tri-reforming, autothermal reforming, steam- CO_2 reforming) of CMM or AMM into a hydrogen-containing gas [9, 10]. The application of effective catalysts ensures practical feasibility of thermodynamically permitted processes and achievement of the equilibrium parameters of the reaction. However, in [10], the autothermal reforming of CMM ($C_{\text{CH}_4} = 42\%$, $C_{\text{air}} = 58\%$) is carried out by adding a large excess of water ($\text{H}_2\text{O}/\text{CH}_4 = 3.26$) and despite the high O/C ratio, the catalyst used ($\text{Ni}/\alpha\text{-Al}_2\text{O}_3\text{-CaO}$) contained carbon deposits after the reaction. The development of catalysts that provide high and stable conversion of CMM or AMM of variable composition into demanded products is an important task.

Traditional industrial methane-reforming catalysts are nickel systems on alumina supports containing various additives (magnesium, calcium, potassium, lanthanum) [11]. The advantages of nickel-aluminum system include the availability and high activity of nickel, the thermal stability and ease of modifying aluminum oxide. Thus, nickel and alumina can be selected as the main components of the catalyst for CMM or AMM conversion into hydrogen-containing gas. Since the temporally variable O/C molar ratio is a feature of methane-containing gas of the coal industry, it seems appropriate to include cerium dioxide in the catalyst composition. CeO_2 is characterized by a high oxygen storage capacity and oxygen mobility of the crystal lattice, it is able to store oxygen when it is in excess in the reaction mixture and, conversely, release it when it is deficient [12]. In addition, when metal nanoparticles (clusters) are stabilized on the CeO_2 surface, a developed metal-support interface is formed, the transport of active oxygen species improves, and the rate of deactivation due to coking during the catalytic process decreases [13,14].

It is known that the particle size of nickel is one of the main characteristics that affects the anti-coking properties of the catalyst under the reaction conditions [15, 16]. For example, for Ni/CeO_2 , it is shown that with an increase in the Ni^0 crystallite size (d_{Ni}) from 10 to 20 nm, the rate of carbon deposition at dry reforming of methane (DRM, $\text{CH}_4 + \text{CO}_2 \leftrightarrow 2\text{CO} + 2\text{H}_2$) at $800\text{ }^{\circ}\text{C}$ increases from 1.6 to 20.9 $\text{mgC}/\text{g}_{\text{cat}}\cdot\text{h}$ [15]. With a further

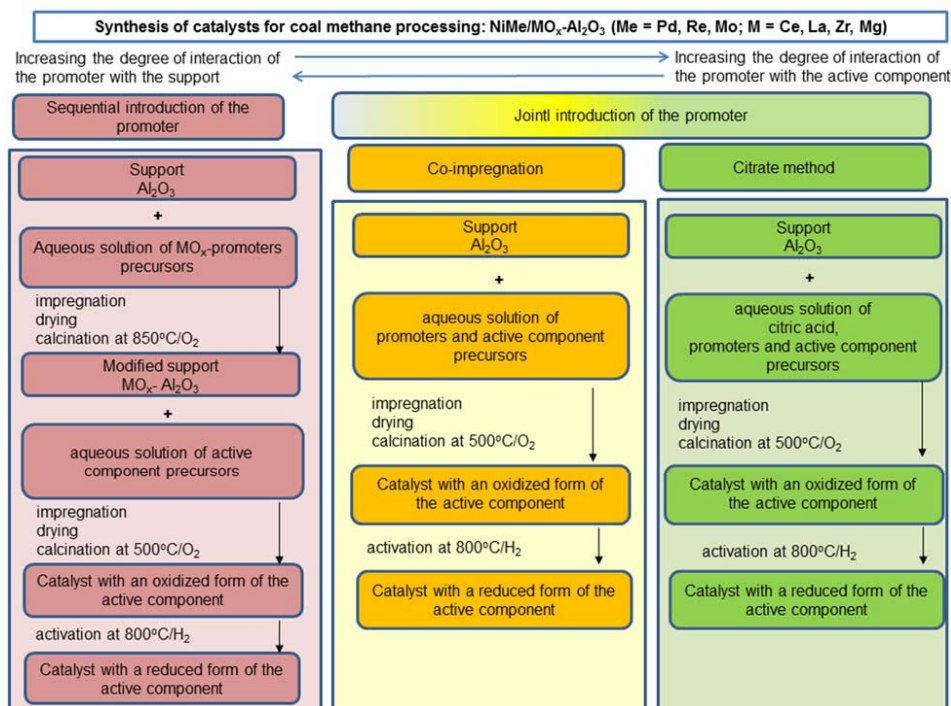


Fig. 1. Scheme of the synthesis of NiMe/MO_x-Al₂O₃ (Me = Pd, Re, Mo; M = Ce, La, Zr, Mg) catalysts for the processing of coal methane.

increase in the Ni⁰ crystallite size, the rate of carbon deposition decreases, amounting to 10.6, 5.9 and 0.3 mgC/g_{cat}·h at d_{Ni} equal to 28, 46 and 116 nm, respectively. For Ni/SiO₂ catalysts with d_{Ni} in the range of 1.2–6.0 nm, the larger the average Ni particle size, the more carbon is formed in both DRM and steam reforming of methane (SRM, CH₄ + H₂O ↔ CO + 3H₂) at 600 °C [16].

In order to obtain supported nickel nanoparticles with a controlled composition and size, various approaches of chemical synthesis are being developed, including tuning the metal–support interaction by modifying the support [17–19] or preparation mode [20–22], achieving a synergistic effect of two elements by designing a catalyst from a bimetallic alloy [23–25], optimization of calcination and activation conditions [15, 26, 27]. Among the modifiers (M = Zr, Gd, La, Mg), La improves the metal–support interaction to the greatest extent, which leads to a decrease in the Ni particle size and an increase in the stability of Ni/Ce_{1-x}M_xO_y and Ni/Ce_{1-x}M_xO_y/Al₂O₃ catalysts during autothermal methane conversion [28]. The exsolution approach in the preparation of the catalyst due to the intensification of metal–support interaction also ensures the stabilization of fine nickel nanoparticles with high anti-coking properties [21]. In the bi-reforming of methane over (CeM)_{0.8}Ni_{0.2}O_y catalysts

(M = Al, La, Mg), the content of coke formed during screening tests (600→850 °C, CH₄:CO₂:H₂O:He = 1:0.8:0.4:2.8) depends on the preparation method and is equal to 0.8 and 20.6 wt.% (M = Al), 6.9 and 26.7 wt.% (M = La), 0.9 and 1.9 wt.% (M = Mg) for samples prepared by the exsolution and impregnation methods, respectively. For bimetallic catalysts, due to the formation of an alloy, Ni-containing particles become more resistant to sintering and re-oxidation [29]. It was established [30] that for Ni/MgAl₂O₄ catalyst for steam reforming of methane, only lower loading of Pt gives synergistic effect with maxima at 0.1 wt.% Pt by increasing the dispersion of the active metal. The principal point is the method for introducing the promoter, which determines its distribution in the bimetallic particle.

Given the above, in our work with an aim to create new highly active and stable catalysts for the complete processing of coal methane, methods for designing catalytic systems are being developed, including the use of the effects of mutual strengthening of the action of metals and modifying the composition of the supports (Fig. 1). Three series of catalysts were obtained, in which the degree of nickel–support interaction increased in the following series of synthesis methods: sequential introduction of the promoter by the impregnation

method < joint introduction of the promoter by the impregnation method < citrate method. Mutual enhancement of the action of metals was achieved by 1) modification of the active component Ni with a second metal (Me = Pd, Re, Mo) or 2) formation of a supported solid solution with an oxide promoter (M = Ce, La, Zr, Mg) followed by its activation in reducing environment.

The aim of this work was to study the effect of the citric acid/(Ce+Ni) molar ratio (0, 0.25, 0.5, 1.0) on the genesis and physicochemical properties of a $\text{Ce}_{0.2}\text{Ni}_{0.8}\text{O}_{1.2}/\text{Al}_2\text{O}_3$ catalysts for reforming coal industry methane to synthesis gas.

2. Experimental

2.1. Catalyst preparation

The $\text{Ce}_{0.2}\text{Ni}_{0.8}\text{O}_{1.2}/\text{Al}_2\text{O}_3$ catalysts were prepared by the citrate sol-gel method. For this, metal nitrate salts ($\text{Ce}(\text{NO}_3)_3 \cdot 6\text{H}_2\text{O}$, $\text{Ni}(\text{NO}_3)_2 \cdot 6\text{H}_2\text{O}$) were added to a solution of citrate acid (CA) in water. Chemicals of 99% purity were purchased from the commercial supplier SoyuzKhimProm and used as such, without any additional purification. The Ni and Ce contents were constant and equal to 10.0 and 5.9 wt.% while the citric acid/M molar ratio (M = Ce + Ni) was varied and equal to 0, 0.25, 0.5 or 1.0. Spherical Al_2O_3 with a grain size of 0.3–0.8 mm was impregnated by the resulting solution. After that, the sample was dried at 90 °C, followed by calcination at a given temperature (500, 700 or 900 °C) for 4 h. Reductive activation of samples was carried out in 30 vol.% $\text{H}_2/70$ vol.% Ar at 800 °C for 1 h.

2.2. Characterization of catalysts

A set of methods was used to study the genesis and physicochemical characteristics of catalysts. A description of devices and conditions for studying materials using physicochemical methods can be found in our earlier publications [21, 31]. The phase evolution was studied by thermogravimetry (TG) and differential thermogravimetry (DTG) with differential thermal analysis (DTA) in air in a simultaneous thermal analyzer (NETZSCH STA 449C, Germany). For the examination of textural properties (S_{BET} – the specific surface area, V_{pore} – total pore volume (V_{pore}), D_{pore} – average pore diameter) N_2 adsorption in an ASAP 2400 auto-

mated volumetric instrument (Micromeritics, the USA) was used. The structural characteristics were investigated by X-ray diffraction with $\text{CoK}\alpha$ radiation ($\lambda = 1.79021 \text{ \AA}$) in an HZG-4C diffractometer (Freiberger Präzisionmechanik, Germany) and Raman spectroscopy using an excitation wavelength of 514.5 nm in a Renishaw Invia Raman spectrometer (Renishaw plc., England). The morphological properties were studied by scanning electron microscopy in a JEOL JSM-6390 LA (JEOL, Japan) electron microscope with an X-ray energy dispersive detector JED 2300. The reducibility of the samples was tested by temperature-programed hydrogen reduction (H_2 -TPR) in a setup equipped with a flow reactor and a thermal conductivity detector.

3. Results and discussion

Figure 2 presents the data of TG, DTG and DTA for dried $\text{Ce}_{0.2}\text{Ni}_{0.8}\text{O}_{1.2}/\text{Al}_2\text{O}_3$ catalysts obtained at different molar ratios of citric acid/(Ni+Ce). When the samples are heated, weight loss is observed, associated with the decomposition of metal salts (nitrate, citrate) and the oxidation of organic matter. The weight loss value increases from 29.8 to 38.4% as the molar ratio increases from 0 to 1. Common for all the samples under study is the weight loss in the low-temperature region ($T < 200 \text{ °C}$) due to water desorption. For the sample obtained without the use of citric acid, two peaks are observed on the DTG curve at temperatures (T_{DTG}) 210 and 285 °C, which are accompanied by endothermic effects and are associated with the decomposition of cerium and nickel nitrates [32, 33], respectively. When a small amount of citric acid (CA/M = 0.25) was added to the impregnating solution, the DTG curve showed one clearly defined peak at $T = 242 \text{ °C}$ and a small shoulder at $T = 270 \text{ °C}$, accompanied by exothermic effects and associated with multi-stage degradation (decomposition, oxidation) of citrate complexes of metals and free citric acid. With an increase in the molar ratio of CA/M from 0.25 to 1, the maxima of T_{DTG} and heat release shifted to the high-temperature region (Fig. 2). Main transformations completed up to 500 °C.

Textural and structural properties of $\text{Ce}_{0.2}\text{Ni}_{0.8}\text{O}_{1.2}/\text{Al}_2\text{O}_3$ catalysts after different treatments are shown in Table 1. The specific surface area and total pore volume of the samples increase with an increase in the CA/M molar ratio. In par-

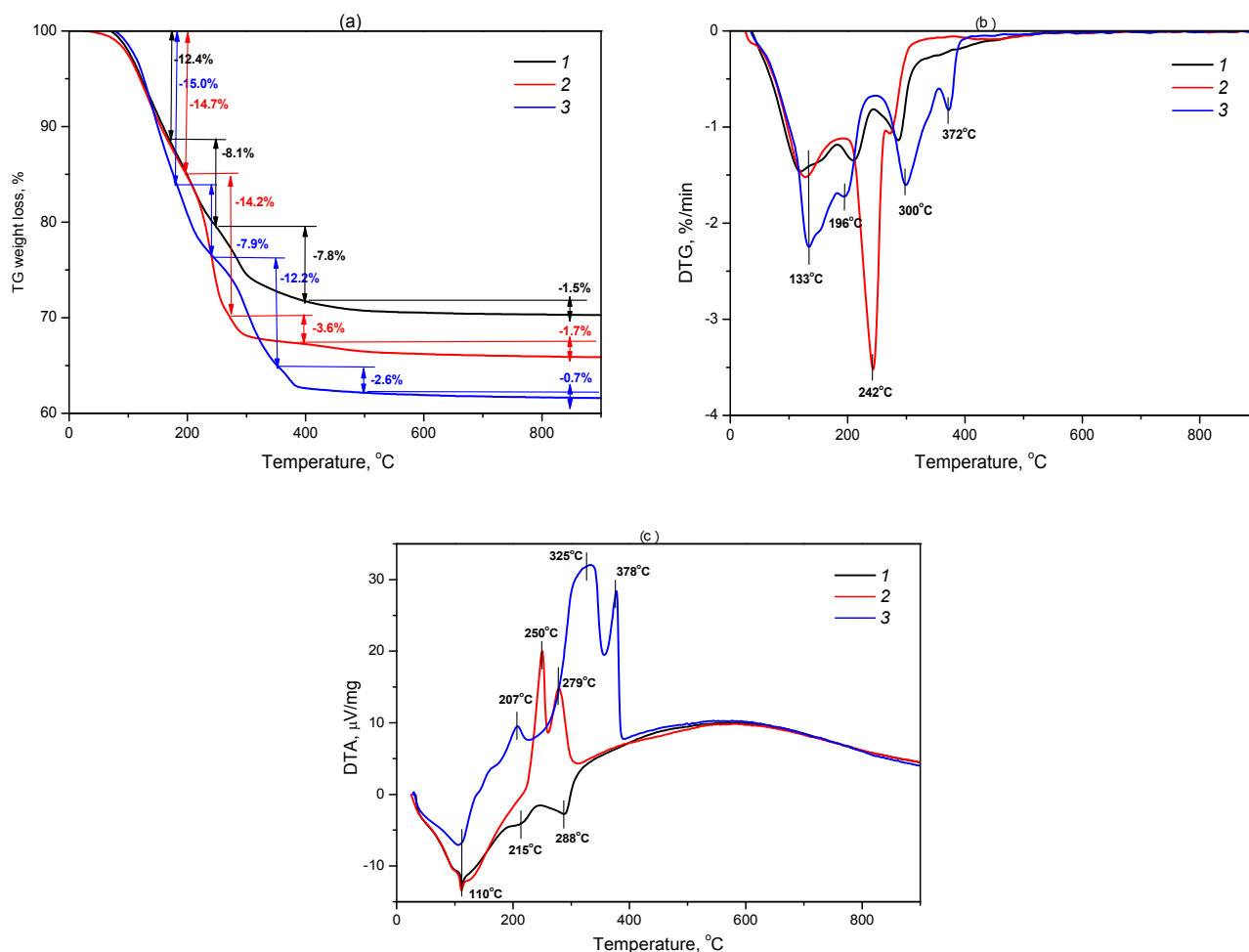


Fig. 2. Data of TG (a), DTG (b) and DTA (c) for dried $\text{Ce}_{0.2}\text{Ni}_{0.8}\text{O}_{1.2}/\text{Al}_2\text{O}_3$ catalysts. The molar ratio of citric acid/(Ni+Ce) was equal to 0 (1), 0.25 (2) and 1.0 (3).

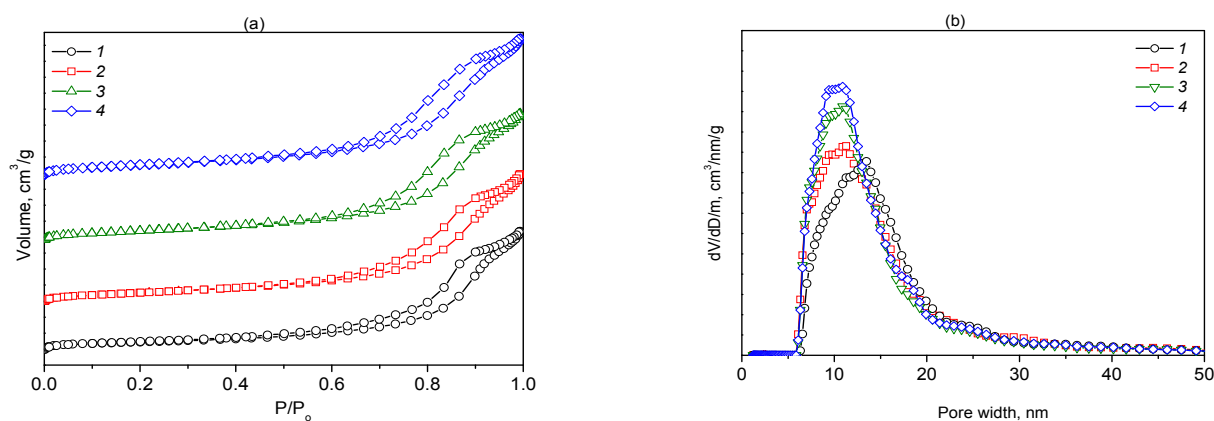


Fig. 3. Data of N_2 sorption (a) and pore size distribution (b) for $\text{Ce}_{0.2}\text{Ni}_{0.8}\text{O}_{1.2}/\text{Al}_2\text{O}_3$ catalysts after calcination in air at 500 °C. The molar ratio of citric acid/(Ni+Ce) was equal to 0 (1), 0.25 (2), 0.5 (3) and 1.0 (4).

ticular, for the catalyst after calcination at 500 °C, S_{BET} changes from 76 to 100 m^2/g when the CA/M value changes from 0 to 1. Regardless of the value of the molar ratio, with an increase in the treatment temperature from 500 to 900 °C, the specific

surface decreased by 20%, while the pore volume remained unchanged. During reductive activation of samples at 800 °C, no more than 10% of the specific surface area was lost which is comparable to calcination in air at 700 °C (Table 1).

Table 1
Textural and structural properties of Ce_{0.2}Ni_{0.8}O_{1.2}/Al₂O₃ catalysts after different treatments*.

CA/M molar ratio	Conditions of treatment	Textural properties			XRD data		I ₅₇₀ /I ₄₆₅
		S _{BET} , m ² /g	V _{pore} , cm ³ /g	D _{pore} , nm	Phase	CSR, nm	
0	500 °C, air	76	0.29	15.5	Al ₂ O ₃ (7.913) CeO ₂ (5.411) NiO	– 7.5 10.0	1.31
	700 °C, air	n.d.	n.d.	n.d.	NiO-Al ₂ O ₃ (7.943) CeO ₂	– 10.0	n.d.
	900 °C, air	n.d.	n.d.	n.d.	NiO-Al ₂ O ₃ (7.965) CeO ₂	– 15.0	n.d.
	800 °C, H ₂	71	0.31	18.0	Al ₂ O ₃ (7.907) CeO ₂ Ni	– 6.5 6.5	–
0.25	500 °C, air	89	0.32	14.2	Al ₂ O ₃ (7.914) CeO ₂ NiO	– – –	7.16
	700 °C, air	82	0.29	14.1	NiO-Al ₂ O ₃ (7.942) CeO ₂	– –	0.30
	900 °C, air	73	0.33	18.3	NiO-Al ₂ O ₃ (7.958) CeO ₂ (5.413)	– 10.0	0.28
	800 °C, H ₂	82	0.33	16.1	Al ₂ O ₃ (7.907) Ni	– –	–
0.5	500 °C, air	95	0.32	13.5	Al ₂ O ₃ (7.914) CeO ₂ NiO	– – –	5.35
	700 °C, air	n.d.	n.d.	n.d.	NiO-Al ₂ O ₃ (7.943) CeO ₂	– 4.0	n.d.
	900 °C, air	n.d.	n.d.	n.d.	NiO-Al ₂ O ₃ (7.965) CeO ₂	– 12.0	n.d.
	800 °C, H ₂	80	0.32	15.9	Al ₂ O ₃ (7.900) Ni	– –	–
1.0	500 °C, air	100	0.34	13.8	Al ₂ O ₃ (7.913) CeO ₂ NiO	– – –	0.96
	700 °C, air	94	0.35	14.9	NiO-Al ₂ O ₃ (7.947) CeO ₂	– 4.0	n.d.
	900 °C, air	80	0.36	18.2	NiO-Al ₂ O ₃ (7.956) CeO ₂	– 12.0	n.d.
	800 °C, H ₂	90	0.31	14.8	Al ₂ O ₃ (7.907) Ni	– –	–

*cell parameters (Å, ±0.003) are indicated in brackets; CSR – the coherent scattering region; I₅₇₀/I₄₆₅ – band intensity ratio at 570 and 465 cm⁻¹ in Raman spectra. ** – no data available.

As follows from the N₂ sorption data, for all study samples, the isotherms are type IV with H₂-type hysteresis (Fig. 3a). According to the IUPAC classification, this is characteristic of mesoporous material. A narrow pore size distribution is observed, the maximum of which shifts to the region of small pores with an increase in the CA/M mo-

lar ratio (Fig. 3b). When varying the conditions of oxidative or reductive heat treatment, the samples retain their mesoporosity (Fig. 4). However, high-temperature treatment leads to an increase in the average pore size. This effect weakens with increasing CA/M molar ratio (Table 1).

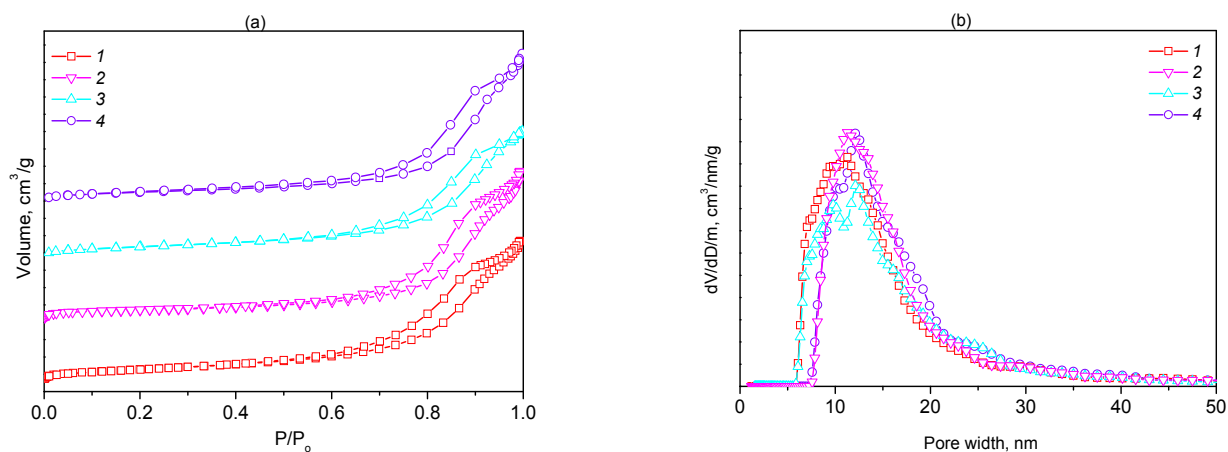


Fig. 4. Data of N_2 sorption (a) and pore size distribution (b) for $Ce_{0.2}Ni_{0.8}O_{1.2}/Al_2O_3$ catalysts after calcination in air at 500 °C (1) and following reductive activation at 800 °C (2), after calcination in air at 700 °C (3) and 900 °C (4). The molar ratio of citric acid/(Ni+Ce) was equal to 0.25.

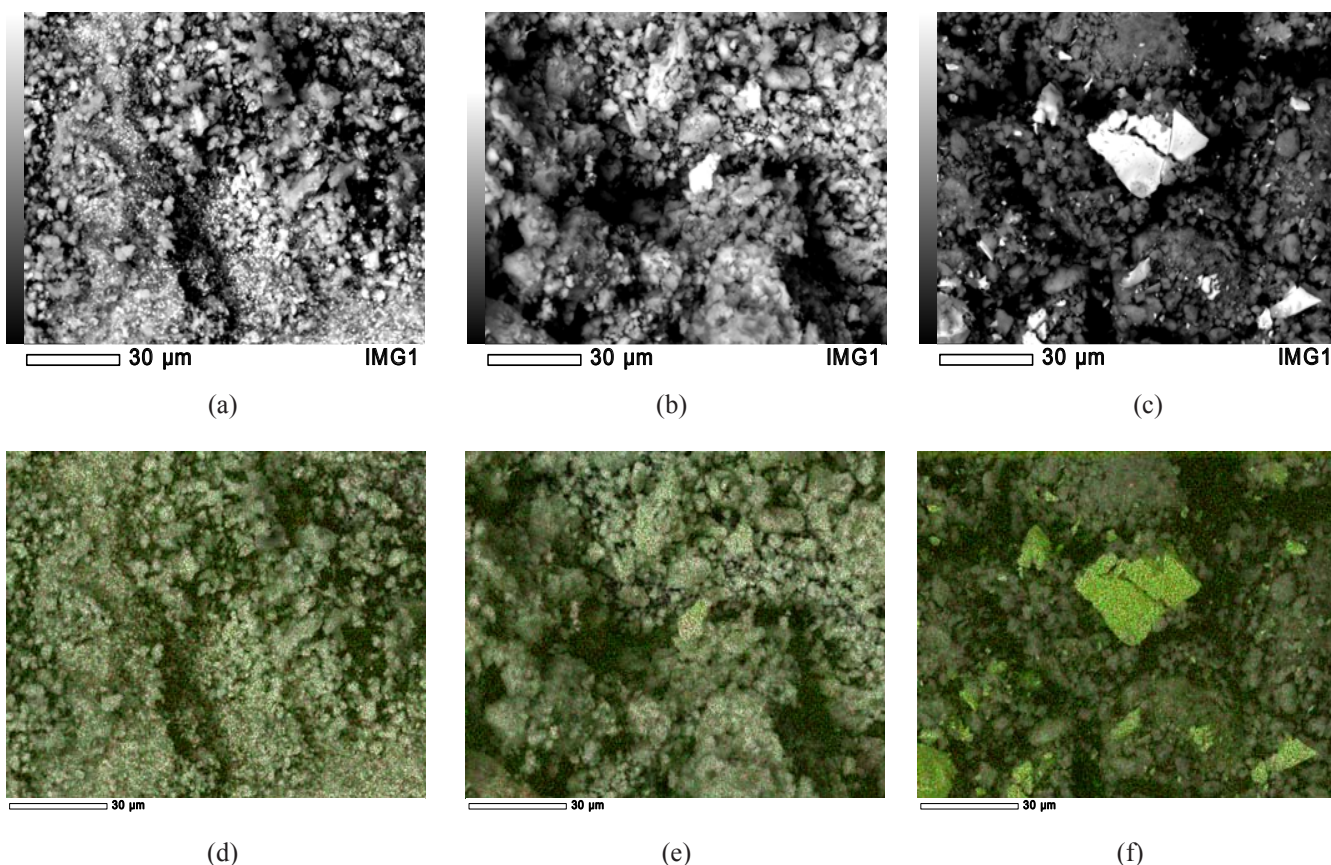


Fig. 5. Electron microscopic images of the surface of $Ce_{0.2}Ni_{0.8}O_{1.2}/Al_2O_3$ catalysts after calcination in air at 500 °C obtained in the modes of registration of backscattered electrons (a, b, c) and characteristic X-ray radiation (K_{Ni} (green), L_{Ce} (red)) (d, e, f). The molar ratio of citric acid/(Ni+Ce) was equal to 0 (a, d), 0.25 (b, e) and 1.0 (c, f).

According to the data of scanning electron microscopy, the samples are agglomerates of irregularly shaped particles (Fig. 5). From the results of EDX mapping, it follows that Ni and Ce elements are evenly distributed throughout the sample.

The XRD pattern of the $Ce_{0.2}Ni_{0.8}O_{1.2}/Al_2O_3$ samples after calcination at 500 °C indicates the presence of $(\gamma+\delta)-Al_2O_3$, CeO_2 and NiO phases (Fig. 6). In the catalysts obtained using citric acid, the supported phases are highly dispersed, which

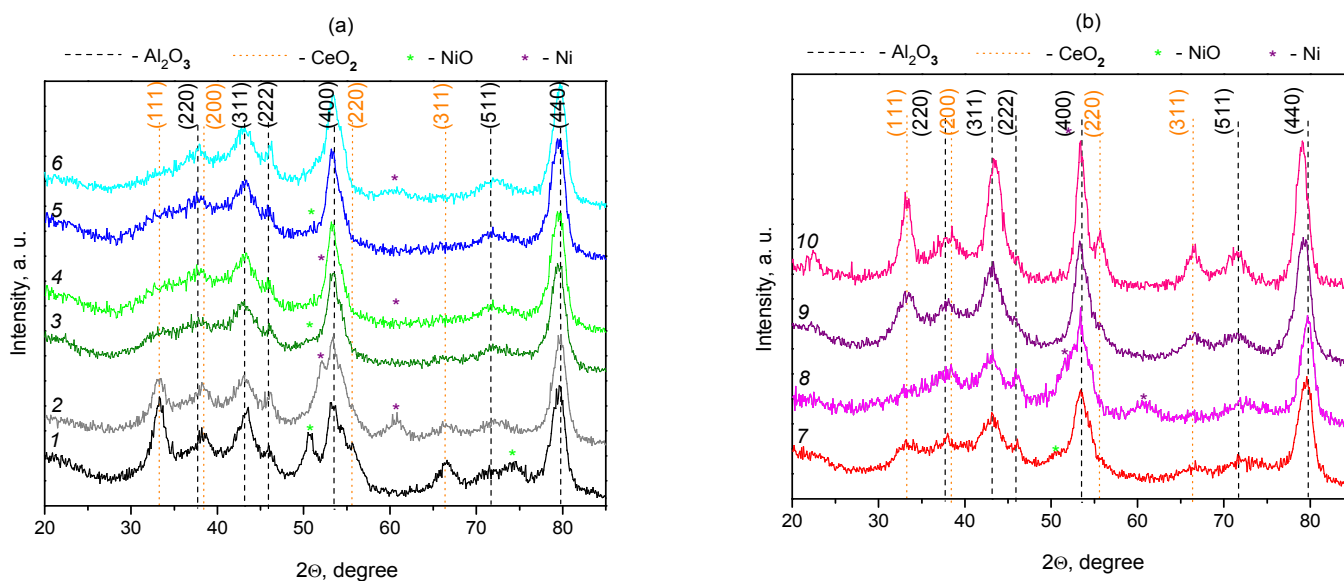


Fig. 6. Data of XRD for $\text{Ce}_{0.2}\text{Ni}_{0.8}\text{O}_{1.2}/\text{Al}_2\text{O}_3$ catalysts after calcination in air at 500 °C (1, 3, 5, 7), and following reductive activation at 800 °C (2, 4, 6, 8), after calcination in air at 700 °C (9) and 900 °C (10). The molar ratio of citric acid/(Ni+Ce) was equal to 0 (1, 2), 0.25 (7–10), 0.5 (3, 4), and 1.0 (5, 6).

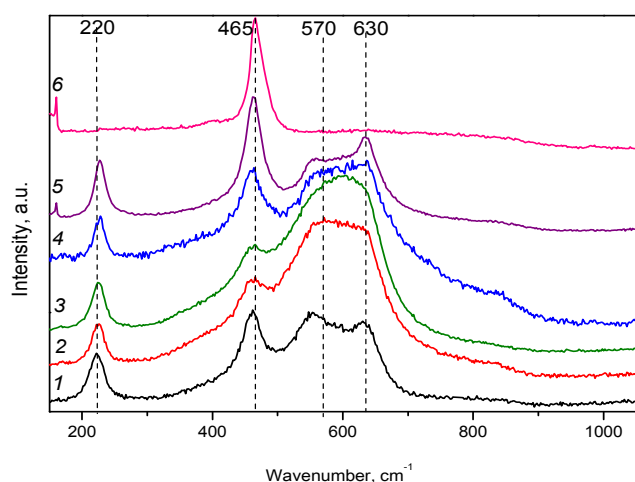


Fig. 7. Data of Raman analysis for $\text{Ce}_{0.2}\text{Ni}_{0.8}\text{O}_{1.2}/\text{Al}_2\text{O}_3$ catalysts after calcination in air at 500 °C (1–4), 700 °C (5) and 900 °C (6). The molar ratio of citric acid/(Ni+Ce) was equal to 0 (1), 0.25 (2, 5, 6), 0.5 (3) and 1.0 (4).

makes it impossible to determine their structural characteristics. For the sample obtained without the addition of citric acid, the average crystallite size of cerium dioxide was 7.5 nm, and that of nickel oxide was 10 nm (Table 1). An increase in the calcination temperature 500→700→900 °C leads to the formation of a Al-Ni-O solid solution based on the spinel structure of alumina, as evidenced by an increase in the formal unit cell parameter of alumina 7.914→7.943→7.965 Å (Table 1). At the

same time, the size of cerium dioxide crystallites remains low and amounts to 10–15 nm. After reductive activation of the samples, highly dispersed nickel particles are formed. As in the samples calcined in air, among the reduced samples, only in the sample obtained without the addition of citric acid was it possible to estimate the average size of metallic Ni⁰ which became equal to 6.5 nm. The re-dispersion of nickel-containing phase is associated with differences in the molar volume of nickel oxide and metallic nickel. The absence of the cerium dioxide phase in the $\text{Ce}_{0.2}\text{Ni}_{0.8}\text{O}_{1.2}/\text{Al}_2\text{O}_3$ samples after activation (Table 1, Fig. 6) may indicate its high dispersion or interaction with alumina to form the highly dispersed CeAlO_3 phase.

The Raman spectroscopic study of $\text{Ce}_{0.2}\text{Ni}_{0.8}\text{O}_{1.2}/\text{Al}_2\text{O}_3$ catalysts revealed that the relative concentration of oxygen vacancies introduced into ceria in order to maintain charge neutrality when Ce^{4+} ions are replaced by cations with different oxidation state depends on the CA/M molar ratio (Table 1, Fig. 7).

The ratio between the integrated area of the D1 peak and the F2g peak (marked as I_{570}/I_{465}) increases from ~1 to 5–7 as the CA/M molar ratio increases from 0 to 0.25–0.5. At a CA/M molar ratio value of 1, I_{570}/I_{465} parameter returns to a value of 1. For bulk CeO_2 support the I_{570}/I_{465} is equal to 0.02. The high value of I_{570}/I_{465} for CeO_2 phase

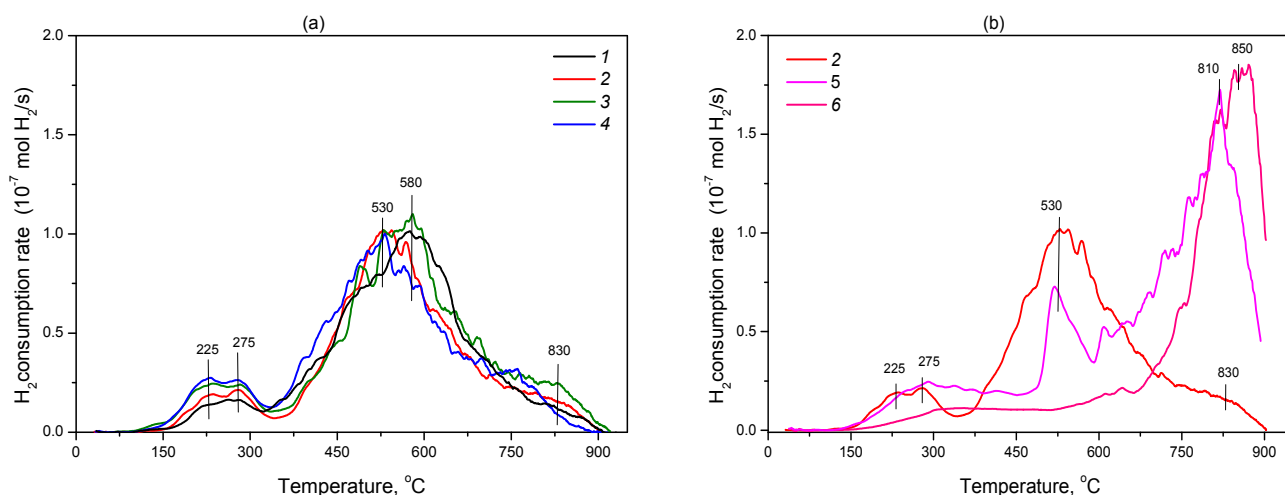


Fig. 8. Data of TPR with hydrogen for $Ce_{0.2}Ni_{0.8}O_{1.2}/Al_2O_3$ catalysts after calcination in air at 500 $^{\circ}C$ (1–4), 700 $^{\circ}C$ (5) and 900 $^{\circ}C$ (6). The molar ratio of citric acid/(Ni+Ce) was equal to 0 (1), 0.25 (2, 5, 6), 0.5 (3) and 1.0 (4).

in the composition of $Ce_{0.2}Ni_{0.8}O_{1.2}/Al_2O_3$ catalysts can indicate that there are replacement of Ce^{4+} cations by Ni^{2+} cations and the formation of Ce-Ni-O solid solution in the prepared samples [34, 35]. The appearance of a well-defined band at 225 cm^{-1} additionally confirms the formation of the Ce-Ni-O solid solution [36]. This process is intensified by the small addition of citric acid.

With an increase in the calcination temperature from 500 to 700–900 $^{\circ}C$, the value of I_{570}/I_{465} decreased significantly and became equal to 0.2–0.3, which indicated a decrease in the concentration of oxygen vacancies. Taking into account the data of X-ray phase analysis, it can be assumed that during high-temperature treatment, the Ce-Ni-O solid solution is destroyed, and Ni^{2+} cations interact with aluminum oxide, forming an Al-Ni-O solid solution based on it.

The study by H_2 -TPR showed that the hydrogen consumption is observed in a wide temperature range of 150–900 $^{\circ}C$, which may indicate the co-existence of various forms of stabilization of metal cations (Fig. 8).

The profile of the TPR curve weakly depends on the CA/M molar ratio (Fig. 8a) but it strongly depends on the calcination temperature (Fig. 8b). As a rule, H_2 consumption in the low-temperature region ($T < 350$ $^{\circ}C$) refers to the reduction of surface [Ni-O-Ce] structures, in the medium-temperature region ($350 < T < 750$ $^{\circ}C$) – to the reduction of Ni^{2+} cations in the bulk of CeO_2 -based solid solution as well as NiO particles, while in the high-temperature region – the reduction of Ce^{4+} cations local-

ized in the volume of particles [21] as well as [Ni-O-Al] structures [37]. After calcination at 500 $^{\circ}C$, the dominant species are Ni^{2+} in the composition of NiO and Ce-Ni-O solid solution. It was found that with an increase in the citric acid/metals molar ratio from 0 to 1, the temperature of maximum H_2 consumption shifts from 580 to 530 $^{\circ}C$ that indicates of the improvement of Ni-containing species reduction (Fig. 8a). An increase in the sample calcination temperature 500 \rightarrow 700 \rightarrow 900 $^{\circ}C$ leads to a decrease in the H_2 consumption in the low- and medium-temperature region, and, on the contrary, an increase in the H_2 consumption at in the high-temperature region (Fig. 8b). Such a behavior of the reducing properties of the samples with an increase in its calcination temperature indicates a decrease in the fraction of [Ni-O-Ce] and NiO species and an increase in the [Ni-O-Al] structures [37], which is in agreement with the XRD results. Note, according to the TPR data (Fig. 8), the appropriate temperature for the reductive activation of the $Ce_{0.2}Ni_{0.8}O_{1.2}/Al_2O_3$ catalysts is 800 $^{\circ}C$, which ensures almost complete reduction of the Ni^{2+} cations of the active component.

Thus the value of citric acid/(Ce+Ni) molar ratio (0, 0.25, 0.5, 1.0) affects the genesis and physicochemical properties of prepared $Ce_{0.2}Ni_{0.8}O_{1.2}/Al_2O_3$ catalysts. When using citric acid during catalyst preparation the type of thermal effect that accompanies the decomposition of the precursor of the active component changes from endothermic to exothermic; the specific surface area of the samples increases; the reducibility and dispersion of Ni spe-

cies are enhanced. The XRD, Raman spectroscopy and TPR studies revealed three forms of Ni²⁺ cation stabilization: NiO, Ce-Ni-O solid solution and Al-Ni-O solid solution. The ratio between these phases depends on the CA/M molar ratio and the temperature of calcination. The citric acid/(Ce+Ni) molar ratio of 0.25–0.5 promotes the formation of Ce-Ni-O solid solution supported on alumina. Such a catalyst is characterized by the small particle size of CeO₂-based phase that increases the availability of oxygen vacancies during catalytic reactions [38] and nanosized particles of Ni, whose reduced size ensures the presence of high concentration of atoms with low coordination number and, accordingly, increased activity [39]. An increase in the calcination temperature from 500 to 900 °C contributes to the stabilization of Ni²⁺ in the [Ni-O-Al] structures, which leads to a slight deterioration in the textural properties of the samples and a significant difficulty in their reducibility. Taking into account the improvement in the physicochemical properties of Ce_{0.2}Ni_{0.8}O_{1.2}/Al₂O₃ samples obtained at CA/M = 0.25–0.5 and calcination at 500 °C, one can expect their excellent functional properties in catalytic processes for the conversion of coal industry methane into valuable products.

4. Conclusions

Different synthesis approaches were considered for the design of highly active and stable Ni catalysts for the conversion of coal industry methane into valuable products. The series of Ce_{0.2}Ni_{0.8}O_{1.2}/Al₂O₃ catalysts were obtained by citrate sol-gel method at variation of citric acid/(Ce+Ni) molar ratio (0, 0.25, 0.5, 1.0) and calcination temperature (500, 700, 900 °C). The samples after different stages of thermal treatment (drying, calcination, activation) were characterized by a group of methods (thermal analysis, N₂ adsorption, X-ray diffraction, scanning electron microscopy, temperature-programed hydrogen reduction). It was found that with an increase in the citric acid/metals molar ratio from 0 to 1, the specific surface area increased from 76 to 100 m²/g, average particle size of Ni active component decreased from 10 to 5 nm and temperature of maximum H₂ consumption decreased from 580 to 530 °C. For catalysts calcined in air at 500 °C, it was shown that Ni²⁺ cations were stabilized in NiO or in the Ce-Ni-O solid solution. The proportion of the latter was

maximum at citric acid/metal molar ratio equal to 0.25, which was chosen as the optimal value. An increase in the calcination temperature from 500 to 900 °C contributed to the stabilization of Ni²⁺ in the Al-Ni-O solid solution, which led to a slight deterioration in the textural properties of the samples and a significant difficulty in their reducibility. Ce_{0.2}Ni_{0.8}O_{1.2}/Al₂O₃ samples with well-dispersed Ni⁰ nanoparticles of ~7 nm in size were formed upon reductive activation at 800 °C. They are expected to exhibit high activity in reforming coal industry methane into synthesis gas.

Funding

The investigation was carried out with support from the Russian Science Foundation under Project No. 22-13-20040, <https://rscf.ru/project/22-13-20040/> and from the Region – the Kemerovo Region – Kuzbass.

Acknowledgments

The authors are grateful to Dr. A.A. Pochtar, Dr. A.A. Leonova, Dr. S.A. Yashnik and Dr. V.A. Ushakov for help with catalyst characterization.

References

- [1]. Statistical Review of World Energy, 2021. <https://www.bp.com/content/dam/bp/business-sites/en/global/corporate/pdfs/energy-economics/statistical-review/bp-stats-review-2021-full-report.pdf>
- [2]. D. Strapoć, F.W. Picardal, C. Turich, et al., *Appl. Environ. Microbiol.* 74 (2008) 2424–2432. DOI: [10.1128/AEM.02341-07](https://doi.org/10.1128/AEM.02341-07)
- [3]. T.A. Moore, *Int. J. Coal Geol.* 101 (2012) 36–81. DOI: [10.1016/j.coal.2012.05.011](https://doi.org/10.1016/j.coal.2012.05.011)
- [4]. B. Wang, Y. Wang, X. Cui, et al., *Biotechnol. Biofuels.* 12 (2019). DOI: [10.1186/s13068-019-1572-y](https://doi.org/10.1186/s13068-019-1572-y)
- [5]. B. Saha, A.S. Patra, A.K. Mukherjee, *J. Mol. Graph. Model.* 106 (2021) 107868. DOI: [10.1016/j.jmgm.2021.107868](https://doi.org/10.1016/j.jmgm.2021.107868)
- [6]. D. Hong, L. Liu, C. Wang, et al., *Fuel* 300 (2021) 120972. DOI: [10.1016/j.fuel.2021.120972](https://doi.org/10.1016/j.fuel.2021.120972)
- [7]. N. Kholod, M. Evans, R.C. Pilcher, et al., *J. Clean. Prod.* 256 (2020) 120489. DOI: [10.1016/j.jclepro.2020.120489](https://doi.org/10.1016/j.jclepro.2020.120489)
- [8]. E.V. Matus, Z.R. Ismagilov, *Eurasian Chem.-Technol. J.* 24 (2022) 203–214. DOI: [10.18321/ectj1433](https://doi.org/10.18321/ectj1433)

- [9]. E.V. Matus, I.Z. Ismagilov, E.S. Mikhaylova, Z.R. Ismagilov, *Eurasian Chem.-Technol. J.* 24 (2022) 69–91. DOI: [10.18321/ectj1320](https://doi.org/10.18321/ectj1320)
- [10]. S. Wang, X. Wang, S. Gao, et al., *Greenhouse Gas Sci Technol.* 7 (2017) 29–39. DOI: [10.1002/ghg.1613](https://doi.org/10.1002/ghg.1613)
- [11]. L.G. Pinaeva, A.S. Noskov, *Kataliz v promyshlennosti* 21 (2021) 308–330 (in Russ.). DOI: [10.18412/1816-0387-2021-5-308-330](https://doi.org/10.18412/1816-0387-2021-5-308-330)
- [12]. T. Montini, M. Melchionna, M. Monai, P. Fornasiero, *Chem. Rev.* 116 (2016) 5987–6041. DOI: [10.1021/acs.chemrev.5b00603](https://doi.org/10.1021/acs.chemrev.5b00603)
- [13]. V.H. Mueller, M.P. Duduković, C.S. Lo, *Appl. Catal. A Gen.* 488 (2014) 138–147. DOI: [10.1016/j.apcata.2014.09.021](https://doi.org/10.1016/j.apcata.2014.09.021)
- [14]. J.A. Rodriguez, D.C. Grinter, Z. Liu, et al., *Chem. Soc. Rev.* 46 (2017) 1824–1841. DOI: [10.1039/c6cs00863a](https://doi.org/10.1039/c6cs00863a)
- [15]. R.O. da Fonseca, A.R. Pongeggi, R.C. Rabelo-Neto, R.C.C. Simões, L.V. Mattos, F.B. Noronha, *J. CO2 Util.* 57 (2022). DOI: [10.1016/j.jcou.2021.101880](https://doi.org/10.1016/j.jcou.2021.101880)
- [16]. C. Vogt, J. Kranenborg, M. Monai, B.M. Weckhuysen, *ACS Catal.* 10 (2020) 1428–1438. DOI: [10.1021/acscatal.9b04193](https://doi.org/10.1021/acscatal.9b04193)
- [17]. E.V. Matus, L.B. Okhlopkova, O.B. Sukhova, et al., *J. Nanoparticle Res.* 21 (2019) 11. DOI: [10.1007/s11051-018-4454-5](https://doi.org/10.1007/s11051-018-4454-5)
- [18]. Y.Lv, Z. Xin, X. Meng, et al., *Appl. Catal. A Gen.* 543 (2017) 125–132. DOI: [10.1016/j.apcata.2017.05.038](https://doi.org/10.1016/j.apcata.2017.05.038)
- [19]. E.V. Matus, S.D. Vasiliev, I.Z. Ismagilov, et al., *Chem. Sustain. Dev.* 28 (2020) 403–411. DOI: [10.15372/csd2020246](https://doi.org/10.15372/csd2020246)
- [20]. E.V. Matus, D.V. Nefedova, O.B. Sukhova, et al., *Kinet. Catal.* 60 (2019) 496–507. DOI: [10.1134/S0023158419040074](https://doi.org/10.1134/S0023158419040074)
- [21]. E. Matus, O. Sukhova, M. Kerzhentsev, et al., *Catalysts* 12 (2022) 1493. DOI: [10.3390/CATAL12121493](https://doi.org/10.3390/CATAL12121493)
- [22]. P. Mäki-Arvela, D.Y. Murzin, *Appl. Catal. A Gen.* 451 (2013) 251–281. DOI: [10.1016/j.apcata.2012.10.012](https://doi.org/10.1016/j.apcata.2012.10.012)
- [23]. I.Z. Ismagilov, A.V. Vosmerikov, L.L. Korobitsyna, et al., *Eurasian Chem.-Technol. J.* 23 (2021) 147–168. DOI: [10.18321/ectj1099](https://doi.org/10.18321/ectj1099)
- [24]. L. Huang, D. Li, D. Tian, et al., *Energy Fuels* 36 (2022) 5102–5151. DOI: [10.1021/acs.energyfuels.2c00523](https://doi.org/10.1021/acs.energyfuels.2c00523)
- [25]. S. Saeedi, X.T. Nguyen, F. Bossola, et al., *Catalysts* 13 (2023) 379. DOI: [10.3390/catal13020379](https://doi.org/10.3390/catal13020379)
- [26]. J. Juan-Juan, M.C. Román-Martínez, M.J. Illán-Gómez, *Appl. Catal. A Gen.* 355 (2009) 27–32. DOI: [10.1016/j.apcata.2008.10.058](https://doi.org/10.1016/j.apcata.2008.10.058)
- [27]. S. Katheria, A. Gupta, G. Deo, D. Kunzru, *Int. J. Hydrogen Energy* 41 (2016) 14123–14132. DOI: [10.1016/j.ijhydene.2016.05.109](https://doi.org/10.1016/j.ijhydene.2016.05.109)
- [28]. Z.R. Ismagilov, E.V. Matus, I.Z. Ismagilov, et al., *Catal. Today* (2019) 166–182. DOI: [10.1016/j.cattod.2018.06.035](https://doi.org/10.1016/j.cattod.2018.06.035)
- [29]. E.V. Matus, I.Z. Ismagilov, S.A. Yashnik, et al., *Int. J. Hydrogen Energy* 45 (2020) 33352–33369. DOI: [10.1016/j.ijhydene.2020.09.011](https://doi.org/10.1016/j.ijhydene.2020.09.011)
- [30]. V.K. Jaiswar, S. Katheria, G. Deo, D. Kunzru, *Int. J. Hydrogen Energy* 42 (2017) 18968–18976. DOI: [10.1016/j.ijhydene.2017.06.096](https://doi.org/10.1016/j.ijhydene.2017.06.096)
- [31]. E. Matus, M. Kerzhentsev, I. Ismagilov, et al., *Energies* 16 (2023). DOI: [10.3390/en16072993](https://doi.org/10.3390/en16072993)
- [32]. C.A. Strydom, C.P.J. van Vuuren, *J. Therm. Anal.* 32 (1987) 157–160. DOI: [10.1007/BF01914558](https://doi.org/10.1007/BF01914558)
- [33]. B. Małecka, A. Łącz, E. Drozd, A. Małecki, *J. Therm. Anal. Calorim.* 119 (2015) 1053–1061. DOI: [10.1007/s10973-014-4262-9](https://doi.org/10.1007/s10973-014-4262-9)
- [34]. L. Li, F. Chen, J.-Q. Lu, M.-F. Luo, *J. Phys. Chem. A* 115 (2011) 7972–7977. DOI: [10.1021/jp203921m](https://doi.org/10.1021/jp203921m)
- [35]. M. Guo, J. Lu, Y. Wu, Y. Wang, M. Luo, *Langmuir* 27 (2011) 3872–3877. DOI: [10.1021/la200292f](https://doi.org/10.1021/la200292f)
- [36]. N. Yisup, Y. Cao, W.L. Feng, W.L. Dai, K.N. Fan, *Catal. Lett.* 99 (2005) 207–213. DOI: [10.1007/s10562-005-2121-9](https://doi.org/10.1007/s10562-005-2121-9)
- [37]. C. Jiménez-González, Z. Boukha, B. De Rivas, et al., *Applied Catal. A Gen.* 466 (2013) 9–20. DOI: [10.1016/j.apcata.2013.06.017](https://doi.org/10.1016/j.apcata.2013.06.017)
- [38]. Anushree, S. Kumar, C. Sharma, *Catal. Sci. Technol.* 6 (2016) 2101–2111. DOI: [10.1039/c5cy01083g](https://doi.org/10.1039/c5cy01083g)
- [39]. Y. Dai, P. Lu, Z. Cao, C.T. Campbell, Y. Xia, *Chem. Soc. Rev.* 47 (2018) 4314–4331. DOI: [10.1039/c7cs00650k](https://doi.org/10.1039/c7cs00650k)